Soham S. Mujumdar
Graduate Student
Department of Mechanical Science and Engineering,
University of Illinois at Urbana-Champaign,
Champaign, IL 61801
e-mail: mujumda2@illinois.edu

Davide Curreli
Assistant Professor
Department of Nuclear, Plasma and Radiological Engineering,
University of Illinois at Urbana-Champaign,
Champaign, IL 61801
e-mail: dcurreli@illinois.edu

Shiv G. Kapoor[1]
Professor
Department of Mechanical Science and Engineering,
University of Illinois at Urbana-Champaign,
Champaign, IL 61801
e-mail: sgkapoor@illinois.edu

David Ruzic
Professor
Center for Plasma-Material Interactions,
Department of Nuclear, Plasma and Radiological Engineering,
University of Illinois at Urbana-Champaign,
Champaign, IL 61801
e-mail: druzic@illinois.edu

A Model of Micro Electro-Discharge Machining Plasma Discharge in Deionized Water

For successful commercial adaptation of the μ-EDM (micro electro-discharge machining) process, there is a need to increase the process efficiency by understanding the process mechanism. This paper presents a model of the plasma discharge phase of a single discharge μ-EDM event in deionized water. The plasma discharge is modeled using global model approach in which the plasma is assumed to be spatially uniform, and equations of mass and energy conservation are solved simultaneously along with the dynamics of the plasma bubble growth. Given the input discharge voltage, current and the discharge gap, complete temporal description of the μ-EDM plasma during the discharge time is obtained in terms of the composition of the plasma, temperature of electrons and other species, radius of the plasma bubble and the plasma pressure. For input electric field in the range of 10–2000 MV/m and discharge gap in the range of 0.5–20 μm, time-averaged electron density of $3.88 \times 10^{24} m^{-3} - 30.33 \times 10^{24} m^{-3}$ *and time-averaged electron temperature of 11,013–29,864 K are predicted. Experimental conditions are simulated and validated against the spectroscopic data from the literature. The output from this model can be used to obtain the amount of heat flux transferred to the electrodes during the μ-EDM process.* [DOI: 10.1115/1.4026298]

1 Introduction

Electrodischarge machining (EDM) is a process in which the material is removed by repeated electrical discharges between the electrodes in presence of a dielectric. μ-EDM is an adaptation of the EDM for removing material in the subgrain size range (0.1–10 μm). The technology has found its applications in many industries due to its ability to machine a range of materials irrespective of their hardness and produce complex geometries with good surface finish. Despite the advantages, the applications of the μ-EDM process have been limited by its slow material removal rate (0.6–6.0 mm^3/h) and low process efficiency in terms of energy utilization. In order to make the μ-EDM process commercially viable, there is a significant need to understand the underlying process mechanism, and thereafter, apply suitable technologies to increase the efficiency of the process. In μ-EDM, the thermal energy required for electrode erosion is supplied by the plasma channel formed in the interelectrode gap. Therefore, modeling the physics of the μ-EDM plasma discharge is an essential step toward understanding the material removal mechanism in the μ-EDM process.

In the EDM process, the dielectric between the electrodes undergoes electrical breakdown under application of electric field greater than its breakdown strength. The mechanism of the breakdown of the dielectric is argued to be different for macroscale EDM versus μ-EDM due to shorter breakdown timescales observed in μ-EDM process [1–3]. However, the basic physics of the plasma discharge stage that follows the breakdown is similar for both macro and μ-EDM process. Most of the studies carried out on the EDM process have been experimental in nature and only a few EDM plasma models exist in the literature. One of the first theoretical studies of EDM plasma dynamics was carried out by Eckman and Williams [4] in which the plasma is modeled as a radially expanding cylindrical column in liquid nitrogen dielectric using one-dimensional Navier–Stokes equation. In this study, the relationships between the plasma characteristics such as the electron density, electron temperature, and input power are obtained by quasi-equilibrium approximations. However, the electron temperature and plasma pressures are found to be much higher than the experimentally observed values. Eubank et al. [5] proposed a variable mass, cylindrical plasma model for conventional EDM in water in which the mass and energy balance equations were solved together with the expanding plasma dynamics. Thermophysical properties of the plasma were derived by assuming it to be a perfect-gas mixture. Dhanik and Joshi [1] modeled a single discharge of μ-EDM process in water as a cylindrical plasma column similar to Eubank et al. but also incorporated mechanism of initial breakdown of the dielectric, and nucleation in their model. However, these models assume thermal equilibrium between electrons, ions, and neutrals throughout the discharge period and require the knowledge of thermophysical properties of the plasma mixture as a function of temperature and pressure in advance. These models also fail to provide the understanding of the complex plasma chemistry in terms of generation and loss of different species in the plasma by various chemical reactions and their effect on the evolution of plasma temperature,

[1]Corresponding author.

Contributed by the Manufacturing Engineering Division of ASME for publication in the Journal of Manufacturing Science and Engineering. Manuscript received August 2, 2013; final manuscript received December 11, 2013; published online March 26, 2014. Assoc. Editor: Y.B. Guo.

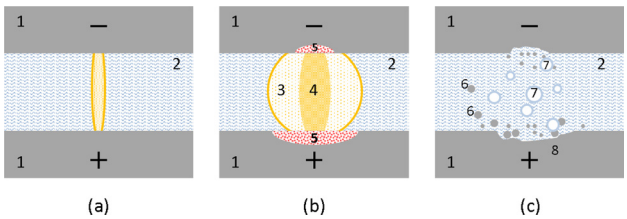

Fig. 1 Schematic of a single discharge of μ-EDM process showing three main phases: (*a*) Dielectric breakdown phase, (*b*) discharge phase, and (*c*) postdischarge phase (1: Electrodes, 2: Dielectric, 3: Vapor bubble, 4: Plasma discharge column, 5: Melt-pool, 6: Debris, 7: Bubbles, 8: Crater)

pressure, and radius. Another drawback of these models is the assumption of a cylindrical plasma column compared to the spherical-shaped geometry of the discharge observed experimentally [6,7]. Therefore, a comprehensive model of μ-EDM plasma is required with emphasis on the complex chemistry of H_2O plasma that presents a clear understanding of the interaction between the high energy electrons and heavy ions/neutrals to eventually reach a common equilibrium temperature.

The purpose of this paper is to develop theoretical understanding of the process mechanism that will provide paths for enhanced efficiency of the μ-EDM process by increasing the material removal rate. The energy and the forces that drive the material removal process are provided by the plasma created in the interelectrode gap. Due to the lack of knowledge of the μ-EDM plasma physics, empirical approach based on the input voltage and the current is used by most of the existing μ-EDM material removal models to estimate the plasma heat flux and the radius. By modeling the plasma, one would be able to predict the plasma characteristics that influence the material removal process, viz., the size of the plasma (radius), the heat flux transferred to the electrodes, and the pressure force exerted on electrode surfaces. Deionized (DI) water is considered as an dielectric for the model as it is one of the most commonly used dielectric for the EDM process [6,8]. The global plasma model approach [9–11] is used to model the plasma, which assumes uniform spatial distributions of plasma characteristics and involves simple governing equations of conservation of mass and energy to estimate the time-transients. The effect of the plasma dynamics during the discharge is also incorporated in the model by coupling the global model with the equations for growth of the plasma-vapor bubble typically observed during an EDM discharge [8,12,13].

The rest of this paper is divided into four sections. In Sec. 2, the modeling approach used to describe the μ-EDM plasma is discussed. Explanation of the model parameters and validation of the model is presented in Sec. 3. The results obtained by the model for a typical μ-EDM discharge as well as for simulation experiments involving different combinations of discharge conditions are discussed in detail in Sec. 4. Finally, the conclusions are presented in Sec. 5.

2 Model Formulation

Figure 1 provides a simple explanation of a single discharge in μ-EDM that can be divided into three phases. First phase is the breakdown phase in which electrically insulating dielectric undergoes electrical breakdown due to application of dc voltage between the electrodes. Due to the voltage applied in a micron-level interelectrode gap, intense electric field is generated in the gap, which triggers ionization of the dielectric liquid forming a plasma channel in the gap. The second phase is the discharge phase in which the already established plasma channel grows radially and a current is established in gap due to the flow of electrons and ions toward the electrodes. It is believed that the bombardment of ions and electrons toward the electrodes results in melting and partly vaporizing the electrode surfaces forming a melt-pool at both the electrodes. As observed by many researchers [12,13], in dielectric like water, the plasma channel is often surrounded by a vapor bubble that expands radially outward due to increasing pressure from the plasma during the discharge phase. Finally, in the third phase when the applied voltage is turned off, the ions and electrons recombine and dielectric strength is recovered. During this phase, the plasma implodes due to pressure exerted by the surrounding dielectric and produces an ejection force on the melt-pool created on the electrode surfaces. This results in removal of the electrode material in forms of small debris particles leaving a small crater at the electrode surface.

The model presented in this paper describes the discharge phase of a single μ-EDM discharge event using a global modeling approach. It is essentially a zero-dimensional model, where spatial variations of the plasma characteristics like density and temperature are ignored to present first-order approximation of the system [11]. Also, a global model does not require much of the computational resources compared to particle-in-cell or fluid models [14]. Figure 2 presents an overview of the model used in this research. As shown in Fig. 2, the model consists of three submodules, viz., plasma chemistry that solves the reaction kinetics involving ionization, dissociation, and recombination reactions; power balance that solves for the temperature of the plasma; and bubble dynamics module that gives the evolution of plasma geometry during the discharge.

The formulation of the model for μ-EDM plasma is discussed further in detail in remaining of this section. Section 2.1 lists the assumptions of the model. The chemistry of H_2O plasma is explained in Sec. 2.2. Power balance equations for the species of interests are presented in Sec. 2.3 and finally, Sec. 2.4 explains the dynamics of the plasma bubble growth during the discharge.

2.1 Assumptions

(1) A single pulse μ-EDM discharge with parallel plate geometry is considered with deionized water as the dielectric.
(2) In pulsed water discharges, it has been observed that a vapor bubble forms between the electrodes, which subsequently expands and collapses [12,13]. It is assumed that the electrical discharge plasma created in this process is of the shape of a spherical bubble throughout the discharge.

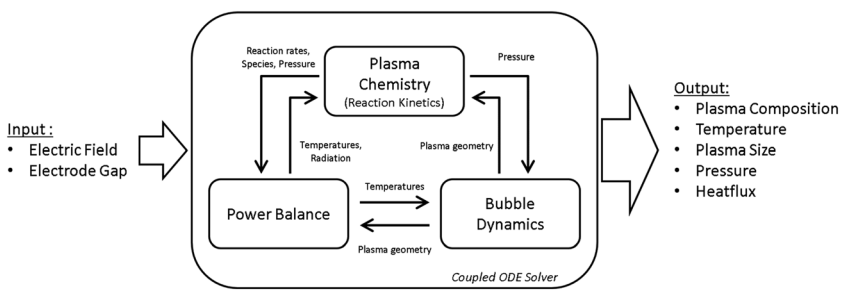

Fig. 2 Global model of μ-EDM process

Table 1 Species included in H_2O plasma model

Neutrals	Positive ions	Negative ions
		e^-
H	H^+	H^-
O	O^+, O^{++}, O^{+++}	O^-
H_2	H_2^+	
O_2	O_2^+	
OH	OH^+	OH^-
H_2O	H_2O^+	
	H_3O^+	

(3) Densities of all the species are assumed to be volume averaged [15]. The energy distribution function of all the species is assumed to be Maxwellian. For a plasma with such high density ($\approx 10^{23}\,m^{-3}$) and pressure (>1 bar) such as μ-EDM plasma, this assumption is well justified [9].
(4) The ions and the neutral species are assumed to share a common temperature (T_g) since they have comparable mass, whereas a separate temperature (T_e) is assigned to the electrons due to their much smaller mass compared to the other species.
(5) Although, the dielectric is considered to be deionized water in this model, it is assumed that a small fraction of electrons and ions are present in the gap at the beginning of the discharge.

2.2 Chemistry of H_2O Plasma. In an electrical discharge in water, the liquid is dissociated and ionized in a number of different species, which can be categorized into electrons, ions, and neutral particles. Depending on the temperature of the reacting species, a large number of reactions are possible producing a significantly large number of different species. Liu et al. [16] have included 46 species and 577 reactions in their global model of $He + H_2O$ glow discharges, which indicates the complexity of chemical processes in a water discharge. It can be computationally overwhelming to consider all the possible reactions to estimate the concentrations of all ionic/neutral species in the plasma. In this research, a set of 41 volumetric reactions involving 19 different species that are sufficient to compute the composition of the significant species in the plasma are selected. Along with the volumetric reactions, some of the species also undergo surface reactions upon bombarding the electrode surfaces. The list of the species considered in this model is tabulated in Table 1 and the complete list of the reactions along with the temperature-dependent reaction rates is listed in Table 6 in the Appendix. The reaction rates are obtained either by integral of the cross-sections from the electron scattering database of Itikawa and Mason [17] over a Maxwellian distribution function, or from the rates listed by Gordon et al. [18]. For computational simplicity, the reactions involving metastable species and complex clusters are neglected. Figure 3 shows plot of temperature-dependent reaction rates of the significant reactions that take place during a discharge in H_2O. As seen from the figure, recombination and charge transfer reactions are most prominent at lower temperatures ($T < 10{,}000$ K), while dissociation and ionization reactions are significant at higher temperatures ($T > 10{,}000$ K) dissociating the H_2O molecule into ions and free electrons. Therefore, in order to form a plasma discharge in deionized water, electron temperature above 10,000 K is typically required in the initial stages of the discharge.

In order to compute the population of each of the species in the plasma, following particle balance equation is solved for each species [16]:

$$\frac{dN_i}{dt} = S_i^V + AS_i^A - A_e\Gamma_{1i} - A_w\Gamma_{2i} - A_l\Gamma_{3i} \tag{1}$$

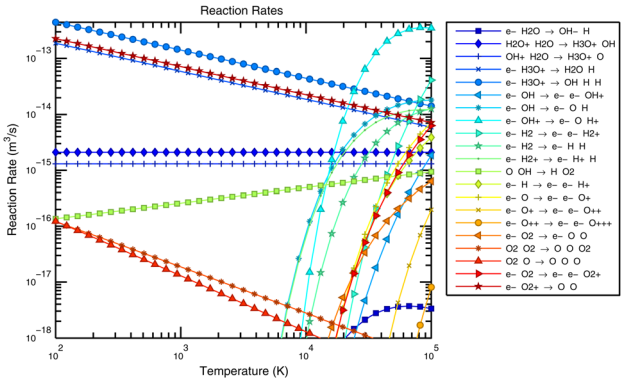

Fig. 3 Plot of temperature-dependent reaction rates of a few significant reactions in H_2O plasma (listed in Table 6 in the Appendix)

where, N_i is the number of atoms/molecules of species i, $S_i^V(s^{-1})$ is the rate of generation/loss of species i due to volumetric reactions, $S_i^A(m^{-2}\,s^{-1})$ is the net generation/loss of species i due to surface reaction at electrode and lateral surface of the plasma, A_e (m^2) is the area of the tool electrode (cathode), A_w (m^2) is the area of the workpiece (anode), A_l (m^2) is the area of the lateral surface of plasma bubble in contact with the dielectric water, A (m^2) is the combined area of electrodes and the lateral surface, V (m^3) the plasma volume, $\Gamma_{1i}(m^{-2}\,s^{-1})$ is the net flux of species i out of plasma through the tool electrode, $\Gamma_{2i}(m^{-2}\,s^{-1})$ is the net flux of species i out of plasma through the workpiece, and $\Gamma_{3i}(m^{-2}\,s^{-1})$ is the net flux of species i out of plasma through the lateral surface of the plasma bubble.

The rate of production of species, S_i^V is equal to [9,16]

$$S_i^V = \frac{1}{V}\sum_{j=1}^{\text{reactions}} \nu_{ij}K_j\left[\prod_{k=1}^{\text{species}}(N_k)^{\alpha_k}\right] \tag{2}$$

where, ν_{ij} is the nondimensional stoichiometric coefficient of species i in reaction j, $K_j(m^3s^{-1})$ is the temperature-dependent rate of reaction j, and α_k is the number of molecules of reactant species k that take part in reaction j. Whenever possible, the rates of the volumetric reactions are computed from the corresponding electron scattering cross-sections by integrating the cross-sections over Maxwellian distribution of electron energy [9,17]. The surface reaction rate, S_i^A, can be computed from the flux (Γ_i) of the reactant species reaching the plasma wall surface with an associated probability β_i of undergoing a surface reaction

$$S_i^A = \beta_i\Gamma_i = \beta_i\frac{1}{4}N_i\left(\frac{8kT_g}{\pi m_i}\right)^{1/2} \tag{3}$$

where, $m_i(Kg)$ is the atomic/molecular mass of the reactant species.

Flux of the neutral species bombarding on the electrodes usually bounces back to the plasma region unless they undergo surface reactions at the plasma wall [16]. The generation/loss of the neutrals at the plasma wall due to surface reactions is already considered as separate term S_i^A as mentioned above. Therefore, for neutrals the flux terms Γ_{1i}, Γ_{2i}, and Γ_{3i} are set to zero.

Usually, the flux terms for negative ions are set to zero as the negative ions are supposed to be trapped by the ambipolar potential field in the plasma [9,16]. The flux of positive ions is calculated by assuming they are driven toward cathode by the uniform axial electric field and a suitable correction factor, h_L, is applied to compensate for the reduced flux due to sharp fall in density near the walls [9,15,16]

$$\Gamma_{1i} = h_L \mu_i \frac{N_i}{V} E \tag{4}$$

where, $\mu_i(\mathrm{m^2V^{-1}s^{-1}})$ is the mobility of ion and $\mathrm{E(Vm^{-1})}$ is the applied electric field. For a cylindrical plasma column, the correction factor along the axial direction (h_L) is [15]

$$h_L = \frac{1 + 3\alpha_{avg}/\gamma}{1 + \alpha_{avg}} \frac{0.86}{\left[3 + L/2\lambda + \left(\frac{0.86 L u_B}{\pi D_a}\right)^2\right]^{1/2}} \tag{5}$$

where, α_{avg} is the ratio of negative ion to electron density, $\gamma = T_e / T_g$, λ (m) is the ion-neutral mean free path, $\mathrm{D_a(m^2\,s^{-1})}$ is the ambipolar diffusion coefficient and $\mathrm{u_B = \sqrt{kT_e/m_i}\,(ms^{-1})}$ is the ion Bohm velocity. Ambipolar diffusion coefficient, D_a is given as [9]

$$D_a = \frac{\mu_i D_e + \mu_e D_i}{\mu_i + \mu_e} \quad \text{with} \quad \mu = \frac{|q|}{m\nu_m}, \quad \text{and,} \quad D = \frac{kT}{m\nu_m} \tag{6}$$

Here, $\mu_e(\mathrm{m^2V^{-1}s^{-1}})$ is the mobility of electrons, and $\mathrm{D_e(m^2s^{-1})}$ and $\mathrm{D_i(m^2s^{-1})}$ are diffusion constant of electron and ions, respectively. The ion-neutral collisional frequency is estimated as

$$\nu_{m,i} = \frac{(8kT_g/\pi m_i)^{1/2}}{\lambda} \quad \text{with} \quad \frac{1}{\lambda} = \frac{N_n}{V}\sigma_{mfp} \tag{7}$$

where, N_n is the population of neutrals and σ_{mfp} ($\mathrm{m^2}$) is the ion-neutral collisional cross-section, suitably chosen to be a large value (10^{-15} $\mathrm{m^2}$) to account for large number of reactions in H_2O plasma.

The flux of electrons at anode can be found directly from the value of electrical current density, J ($\mathrm{Am^{-2}}$), flowing through the plasma. However, the net number of electrons actually lost from the plasma, $(\Gamma A)_e(1/s)$, is calculated by total number of positive ions lost from the plasma (at cathode) in order to maintain quasi-neutrality of the plasma as follows:

$$(\Gamma A)_e = \sum_{i}^{\text{positive ions}} \Gamma_{1i} A_e, \tag{8}$$

In order to solve the particle balance equations, temperature of each of the species is required since the rates of the reactions that consume or generate the species depend on the temperature of reactant species. The temperature of the species is obtained by simultaneously solving power balance equation along with the particle balance.

2.3 Power Balance. Figure 4 represents the energy flow diagram of the system. As seen in the figure, in a typical plasma discharge the electrical power (P_{in}) is directly coupled to the electrons, which in turn transfer it to neutrals and ions through elastic collisions ($Q_{el,e}$) and Coulomb interactions ($Q_{c,e}$) [9]. As the neutrals and ions have comparable mass and are heavier than electrons, a common temperature T_g is assigned to the ensemble of neutrals and ions and a separate temperature T_e is assigned to the electrons. Two separate power balance equations are solved to estimate the evolution of T_e and T_g during the discharge.

2.3.1 Power Balance for Electrons. The power balance equation that governs the electron temperature is [9]

$$\frac{d}{dt}\left(\frac{3}{2}N_e k T_e\right) = P_{in,e} - P_{w,e} - P_{rad,e} - Q_{el,e} - Q_{inel,e} - Q_{c,e} - P_{wall,e} \tag{9}$$

where, $k\,(\mathrm{JK^{-1}})$ is the Boltzman constant, $P_{in}\,(\mathrm{W})$ is the input electrical power given to electrons during the discharge, $P_{w,e}\,(\mathrm{W})$ is the rate of mechanical work done by electrons to expand the bubble, $P_{rad,e}\,(\mathrm{W})$ the radiative power loss from the plasma bubble, $Q_{el,e}\,(\mathrm{W})$ the power lost by electrons in elastic collisions with neutrals and ions, $Q_{inel,e}\,(\mathrm{W})$ the power lost by electrons in process of inelastic collisions with neutrals and ions, and $Q_{c,e}\,(\mathrm{W})$ is the power lost by electrons due to Coulomb interaction between electrons and ions.

P_{in} is calculated based on the applied electric field E as

$$P_{in} = (JE)V \quad \text{with} \quad J = \sigma_{dc}E \tag{10}$$

where, $J\,(\mathrm{Am^{-2}})$ is the plasma current density, $\sigma_{dc}\,(\mathrm{S/m})$ is the dc plasma conductivity in cold plasma approximation [9]

$$\sigma_{dc} = \frac{e^2 N_e}{m_e \nu_{m,e} V} \tag{11}$$

Here, $\nu_{m,e}\,(\mathrm{s^{-1}})$ is the collision frequency of electrons with neutrals.

The power lost by electrons to mechanically expand the bubble, $P_{w,e}$, is

$$P_{w,e} = N_e k T_e \frac{dV}{dt} \tag{12}$$

The radiative power loss, $P_{rad,e}$ is obtained from

$$P_{rad,e} = \varepsilon \sigma_{sb}(T_e^4 - T_a^4)A \tag{13}$$

The emissivity of the plasma (ε) is assumed to be unity in this model.

The power transferred by electrons to the neutrals in process of elastic collisions is written as [9]

$$Q_{el,e} = \frac{1}{V}\sum_{j=1}^{\text{elastic reactions}} \frac{3m_e}{M_j} k(T_e - T_g) K_j \left[\prod_{k=1}^{\text{species}} N_k^{\alpha_k}\right] \tag{14}$$

where, $m_e\,(\mathrm{Kg})$ is the mass of the electron, $M_j\,(\mathrm{Kg})$ is the reduced mass of all the reactants in reaction j, and $T_g\,(\mathrm{K})$ is the temperature of neutral species.

$Q_{inel,e}$ represents the power lost by electrons in inelastic collisions with neutrals and ions [9]

$$Q_{inel,e} = \frac{1}{V}\sum_{j=1}^{\text{inelastic reactions}} E_j K_j \left[\prod_{k=1}^{\text{species}} N_k^{\alpha_k}\right] \tag{15}$$

where, $E_j\,(J)$ is the characteristic energy of reaction j. The characteristic energy has been assumed to be the ionization energy for ionization processes.

The electrons also interact with ions by Coulomb interaction in which rate of energy $Q_{c,e}$ is transferred to ions [19]

$$Q_{c,e} = \frac{2.9 \times 10^{-12}\lambda}{V}\left(\frac{kT_e}{e}\right)^{-\frac{3}{2}} \sum_{j=1}^{\text{ions}} \frac{3m_e}{M_j} k(T_e - T_j) N_e N_j Z_j^2 \tag{16}$$

where, λ is the Coulomb logarithm ($\lambda = \ln\Lambda \approx 10$), e(C) is the elementary charge, $M_j(\mathrm{Kg})$ is the mass of ion j, $T_j(\mathrm{K})$ is the temperature of ion j, which is assumed to be same for all the ions and neutral species (T_g), and Z_j is the charge number of ion j.

The power lost by electrons at the wall is given by [20]

$$P_{wall,e} = \left(\frac{5}{2}kT_e\right)(\Gamma A)_e \tag{17}$$

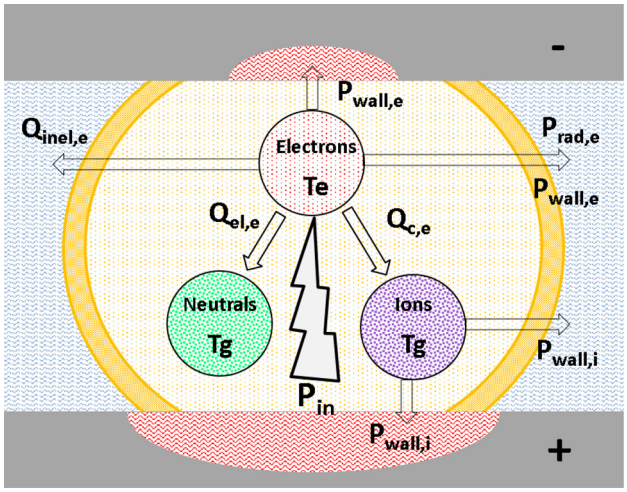

Fig. 4 Energy flow diagram of μ-EDM plasma showing interaction between electrons, ions, and neutral species in an expanding plasma bubble

2.3.2 Power Balance for Ions and Neutrals. Similar to electrons, a separate power balance equation can be written for ions and neutrals

$$\frac{d}{dt}\left(\sum_{\mathrm{i}}^{\text{ions, neutrals}} c_{vi} N_{\mathrm{i}} k T_{\mathrm{g}}\right) = Q_{\mathrm{el,g}} + Q_{\mathrm{c,g}} - P_{\mathrm{w,g}} - P_{\mathrm{wall,i}} \tag{18}$$

where, c_{vi} is the specific heat coefficient of species i, which when multiplied by Boltzman constant (k) gives the specific heat of the gas per molecule under constant volume. The specific heat coefficient is related to the total degree of freedom (f_{i}) for an ideal gas

$$c_{vi} = \frac{f_{\mathrm{i}}}{2} \tag{19}$$

For mono-atomic species there are 3 degrees of freedom. For multi-atomic molecules with n number of atoms per molecule, each atom has 3 degrees of freedom, leading to total $3n$ degrees of freedom for the molecule.

$Q_{\mathrm{el,g}}$ (W) is the power gained by neutral/ion particles in elastic collisions with electrons, $Q_{\mathrm{c,g}}$ (W) the power gained by ions in Coulomb interaction with electrons, $P_{\mathrm{w,g}}$ (W) is the rate of mechanical work done by neutral and ions to expand the bubble, and $P_{\mathrm{wall},i}$ (W) is the power transferred to the plasma walls due to bombardment of ions. Here

$$Q_{\mathrm{el,g}} = Q_{\mathrm{el,e}}, \quad \text{and,} \quad Q_{\mathrm{c,g}} = Q_{\mathrm{c,e}} \tag{20}$$

The rate of mechanical work done by neutrals and ions, $P_{\mathrm{w,g}}$ can be obtained from

$$P_{\mathrm{w,g}} = \sum_{\mathrm{i}}^{\text{ions, neutrals}} N_{\mathrm{i}} k T_{\mathrm{g}} \frac{dV}{dt} \tag{21}$$

The power loss by the ions at the wall is given as [20]

$$P_{\mathrm{wall,i}} = \left(\frac{5}{2} k T_{\mathrm{g}}\right) \sum_{\mathrm{i}}^{\text{ions}} \left(A_{\mathrm{e}} \Gamma_{1\mathrm{i}} + A_{\mathrm{w}} \Gamma_{2\mathrm{i}} + A_{l} \Gamma_{3\mathrm{i}}\right) \tag{22}$$

2.4 Plasma Bubble Growth Model. It has been observed in underwater discharges including μ-EDM that a vapor bubble is formed during initial stages of the discharge containing the plasma and the bubble expands due to increasing internal pressure until it collapses violently when the electrical power is shut off [12]. The spark-generated bubble dynamics for macroscopic underwater discharges has been modeled previously by many researchers [21,22] using Kirkwood-Bethe model, which has been proved very effective. The same model is adopted to describe the bubble dynamics with a spherical-shaped plasma bubble expanding in the radial direction

$$\ddot{R}\left(1 - \frac{\dot{R}}{C}\right) = \frac{\dot{p}}{\rho C}\left(1 - \frac{\dot{R}}{C}\right) + \frac{H}{R}\left(1 + \frac{\dot{R}}{C}\right) - \frac{3\dot{R}^2}{2R}\left(1 - \frac{\dot{R}}{3C}\right) \tag{23}$$

where, R (m) denotes the plasma bubble radius, C (ms^{-1}) is the speed of sound in water, and H(JKg^{-1}) is the specific enthalpy of the bubble wall given as

$$C^2 = n\frac{p+B}{\rho_\infty}, \quad n = 7.15 \quad B = 304.913\,\mathrm{MPa} \tag{24}$$

$$H = \int_{p_\infty}^{p} \frac{dp}{\rho} \tag{25}$$

To evaluate the integral in Eq. (25), Tait's equation of state is used for liquid water density [22]

$$\frac{p+B}{p_\infty + B} = \left(\frac{\rho}{\rho_\infty}\right)^n \tag{26}$$

where, p(Pa) is the pressure outside the bubble wall, ρ(Kgm^{-3}) is the density at pressure p, p_∞(Pa) is the ambient pressure and ρ_∞ (Kgm^{-3}) is the density of water at ambient pressure. Pressure (p) outside the bubble wall is given by pressure balance equation at the bubble wall

$$p = p_B - \frac{2\sigma_s}{R} - \frac{4\mu\dot{R}}{R} \tag{27}$$

where, σ_{s}(Nm^{-1}) is the surface tension of liquid water, μ(Pas) is the dynamic viscosity of the liquid water and p_{B}(Pa) denotes the pressure inside the bubble given by

$$p_B = \frac{N_{\mathrm{e}} k T_{\mathrm{e}}}{V} + \sum_{\mathrm{i}}^{\text{ions, neutrals}} \frac{N_{\mathrm{i}} k T_{\mathrm{g}}}{V} \tag{28}$$

Equations (1), (9), (18), and (23) are solved simultaneously in order to obtain complete description of the μ-EDM plasma in terms of the composition of the plasma, temperature of the plasma, and the radius of the plasma bubble. Heat flux to the electrodes is also an important quantity of interest from the manufacturing point of view. For cathode (tool electrode), the heat flux is due to radiation and bombardment of positive ions

$$Q_{\mathrm{tool}} = Q_{\mathrm{rad}} + \sum_{\mathrm{i}}^{\text{positive ions}} \Gamma_{1\mathrm{i}} \left(\frac{5}{2} k T_{\mathrm{g}}\right) \tag{29}$$

and, for anode (workpiece), the heat flux is due to radiation and electron current

$$Q_{wp} = Q_{\mathrm{rad}} + \frac{J}{\mathrm{e}}\left(\frac{5}{2} k T_{\mathrm{e}}\right) \tag{30}$$

3 Model Evaluation and Validation

The model is evaluated by numerical integration in MATLAB using a stiff ODE solver (ode15s) with relative tolerance of 10^{-6}. To set up the initial conditions for numerical integration of the

Table 2 Constants and material properties [30]

$k = 1.38 \times 10^{-23}\,\mathrm{JK}^{-1}$	$e = 1.6 \times 10^{-19} C$
$\sigma_{sb} = 5.67 \times 10^{-8}\,\mathrm{Wm}^{-2}\mathrm{K}^{-4}$	$T_a = 300\,\mathrm{K}$
$T_b = 373.15\ K$	$T_w = 300\,\mathrm{K}$
$p_\infty = 101325\,\mathrm{Pa}$	$\rho_\infty = 997\,\mathrm{Kgm}^{-3}$
$c_{pw} = 4181, \mathrm{JKg}^{-}\mathrm{K} - 1$	$H_v = 2257 \times 10^3\,\mathrm{JKg}^{-1}$
$\sigma_s = 7.17 \times 10^{-2}\,\mathrm{Nm}^{-1}$	$\mu = 8.592 \times 10^{-4}\,\mathrm{Pas}$

governing equations, it is assumed that at time $t = 0$, the dielectric has undergone a breakdown and a plasma channel has been formed between the interelectrode gap. As the plasma bubble is spherically shaped, initial diameter of the bubble is taken to be equal to the interelectrode gap distance (d) giving us initial condition for the radius of the plasma

$$R_0 = d/2, \quad \dot{R}_0 = 0. \tag{31}$$

Initially, the bubble is composed of the water vapor and a few electrons due to newly formed plasma channel. Therefore, initial condition for the temperature of the ion-gas ensemble (T_g) is chosen as the boiling point of water. The pressure outside the bubble wall can be taken as the atmospheric pressure by neglecting the hydrodynamic pressure from the dielectric and the initial pressure inside the bubble can be derived based on Eq. (28). Thus

$$T_{g0} = T_b, \quad p_{B0} = p_\infty + \frac{2\sigma_s}{R_0} \tag{32}$$

Knowing the initial pressure and temperature, initial population of the water vapor (H_2O) can be found out from the ideal gas law

$$N_{\mathrm{H_2O},0} = \frac{p_{B0} V_0}{k T_{g0}}. \tag{33}$$

Usually, the conductivity of the DI water ranges from 0.1 to 10 μS/cm [23,24]. For electrons, the initial population is calculated based on Eq. (11) corresponding to conductivity of 10 μS/cm and set to be 0.15% of initial population of water vapor. The initial electron temperature is chosen to be equal to the boiling point of water. To maintain quasi-neutrality, initial population of H_2O^+ ions is set equal to the initial population of electrons and population of all other species is assumed to be zero. The constants and material properties used for the simulation are listed in Table 2.

To validate the model, experimental measurements of the plasma characteristics, i.e., plasma composition, temperature and radius over the discharge period are required. However, due to micron-level gaps and short discharge periods, measurement of plasma characteristics in μ-EDM is extremely difficult. As a result, very few experimental μ-EDM plasma characterization studies exist in the literature. To validate the model, the electron temperature and the electron density of the plasma are compared with the experimental work of Nagahanumaiah et al. [25]. The results reported by Nagahanumaiah et al. are based on spectroscopic measurements of the single-discharge experiments, where relative intensities of different spectral lines are measured to find electron temperature and electron density using line-pair method [25]. During the experiments [25], the μ-EDM process parameters, namely, capacitance, electrode size, applied voltage, applied current, and the discharge gap are varied in order to measure the effect of these parameters on the plasma temperature and electron density. However, the model presented here considers only the electric field and the discharge gap as the input parameters, and the value of input power is calculated based on the conductivity of the plasma and the applied electric field. Therefore, to simulate the experimental conditions of applied voltage, a constant electric field in the discharge gap given by $E = V/L$ is assumed. Initially, the current flowing through the plasma can be calculated from the relation $J = \sigma_{\mathrm{dc}} E$; however, when this value surpasses the applied current, it is fixed at the value of the applied current. For each combination of the applied voltage, current, and the gap, the discharge is simulated for the same discharge period of 10 μs as in the experiments. Due to lack of knowledge of the discharge gap used in the referred experiments, two values of the discharge gap (0.5 μm, 1 μm) are considered. The values of the discharge gaps are chosen such that the resulting electric field at these gaps ($E = V/L$) is above the dielectric strength of water, which is taken to be ≈38 MV/m [26]. The dielectric strength of water is the maximum electric field it can withstand without undergoing electric breakdown. The initial population of electrons is taken as 0.15% of the initial population of H_2O vapor, which corresponds to initial conductivity of 10 μS/cm.

Table 3 compares the values of electron temperature and electron density obtained experimentally by Nagahanumaiah et al. against the time-averaged values of electron density and electron temperature obtained by the model presented in this paper. As seen from the table, the values of time-averaged electron temperature predicted by the model range from 6149 K to 7355 K with an average of 6817 K over all the trials and match reasonable well with the corresponding experimental values reported in Ref. [25], which range from 5326 K to 7182 K with an average of 6217 K. The values of the time-averaged electron density predicted by the model range from 7.4×10^{23} to 10.0×10^{23} m^{-3} with an average of 8.9×10^{23} m^{-3} over all the trials, whereas the values of electron density reported in Ref. [25] has an average of 23.9×10^{23} m^{-3}. Note that the electron density predicted by the model is of the same order of magnitude as the experimental value.

4 Results and Discussion

The model of the μ-EDM plasma is used to obtain a complete description of the plasma during the discharge by simulating the evolution of different plasma characteristics, namely, the

Table 3 Comparison of the μ-EDM model with experimental results from literature

			Experimental results [24]			Results from the model (time-averaged[b])	
Voltage (V)	Current (A)	Gap[a] (μm)	Electron temperature (K)	Electron density (10^{23} m^{-3})	Gap (μm)	Electron temperature (K)	Electron density (10^{23} m^{-3})
40	2.0	A	7181.5	24.4	0.5	6148.7	7.5
40	2.0	B	6446.5	17.7	1.0	6668.9	7.4
45	3.0	A	5325.7	46.1	0.5	6789.0	10.0
45	3.0	B	5602.5	15.2	1.0	7354.7	9.6
50	2.5	A	6171.1	18.3	0.5	6691.5	9.6
50	2.5	B	6576.8	21.5	1.0	7250.1	9.2

[a]A < B, exact values of the gap levels have not been reported by the authors.
[b]Average of values taken over the entire discharge duration.

Table 4 Result of the simulation for $E = 100$ MV/m, $L = 1$ μm and $t_d = 5$ μs

Output	Maximum	Mean	Minimum
Electron density (10^{24} m^{-3})	189.30	7.53	0.38
Electron temperature (K)	203,510	14,794	10,215
Ion–gas temperature (K)	201,990	14,791	10,211
Plasma radius(μm)	717		
Plasma pressure (atm)	6133	245	121
Heat flux to workpiece (anode) (10^{10} W/m^2)	24,564	9.44	6.45
Heat flux to tool (cathode) (10^{10} W/m^2)	9736	3.90	6.17

composition of the plasma, temperature of the plasma, radius and velocity of expansion, pressure inside the plasma, and heat flux transferred to the electrodes from the model. The results obtained have been discussed in Secs. 4.1 and 4.2, first, for a case of a typical μ-EDM discharge and then for simulation experiments involving different combinations of applied electric field and gap distance.

4.1 Evolution of the Plasma Characteristics During a Typical Discharge. A typical μ-EDM process is characterized by micron-level interelectrode gaps and microsecond level pulse durations. Therefore, to simulate a typical μ-EDM discharge, electric field (E) of 100 MV/m, gap (L) of 1 μm and discharge time (t_d) of 5 μs are used. Table 4 lists the range and the time-averaged

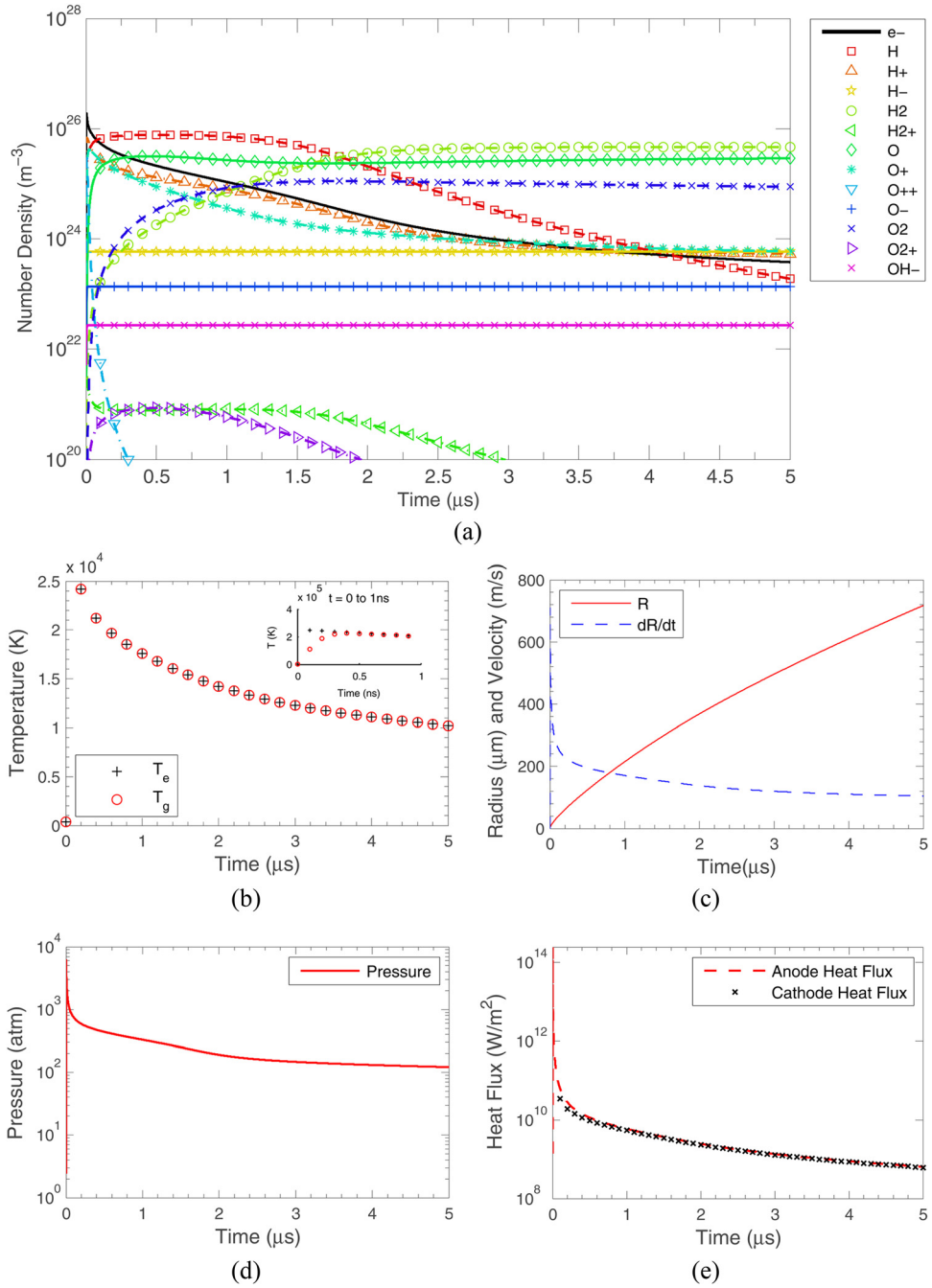

Fig. 5 Evolution of plasma characteristics

values of the plasma characteristics predicted by the model for the typical μ-EDM discharge, while the time evolution of the plasma characteristics are plotted in Fig. 5.

Figure 5(*a*) presents the composition of μ-EDM plasma in terms of the number densities of significant species as a function of time. Out of total 19 species considered in the model, number densities of the species having density greater than 10^{20} m^{-3} have been shown. Evolution of electron temperature and the temperature of ions and neutrals is shown in Fig. 5(*b*), while Fig. 5(*c*) shows the radius and the velocity of expansion of the plasma bubble as a function of time. Since the reaction rates are temperature dependent, the particle balance equation (Eq. (1)) is coupled with the power balance equations for electrons as well as for ions and neutrals (Eqs. (9) and (18)). Furthermore, to calculate the number density of a species from the number of particles, one requires the size of the plasma bubble, which is governed by the Kirkwood-Bethe equation (Eq. (23)). Therefore, one must analyze Figs. 5(*a*)–5(*c*) together in order to understand the time evolution of plasma composition, plasma temperature, and plasma radius and the interdependence of these characteristics on each other.

Initially all the electrical power due to applied electric field is transferred to electrons due to which a sharp increase can be seen in the electron temperature (refer to Fig. 5(*b*)). At higher energies, the electrons collide with the water molecules to cause dissociation and ionization of H_2O into positive ions (H_2O^+, OH^+, O^+, H^+, H_2^+), negative ions (H^-, O^-, OH^-), neutrals (H, H_2, OH, O) and more electrons following reactions 1–11 from Table 6 in the Appendix. In the process of collisions, the electrons also transfer some of their energy to the ions and neutrals, therefore, triggering the increase in the temperature of ions and neutrals. This process of dissociation of water molecule and increase of the plasma temperature (T_e, T_g) takes place within first few subnanoseconds of the discharge duration (see Fig. 5(*b*)). At this point, the thermal equilibrium between swift electrons and heavy ions/neutrals is achieved. Due to sharp increase in the density of species and plasma temperature, the pressure inside the plasma bubble increases as shown in Fig. 5(*d*) following the ideal gas law ($p = NkT/V$). As a consequence of increase in pressure, plasma bubble starts to expand radially as seen in Fig. 5(*c*).

After initial increase in the density, the further evolution in the density of a species is a consequence of the complex chemical kinetics (Table 6 in the Appendix) and expanding plasma radius. For electrons, the rate of generation of electrons through volumetric reactions does not reach high enough value to compensate for decrease in the electron density due to increase in plasma volume and loss of electrons at the wall. Therefore, the electron density decays slowly from initial value of 1.89×10^{26} m^{-3} to final value of 3.8×10^{23} m^{-3} as seen from Fig. 5(*a*). Similar trend is observed for the positive ions (H^+, H_2^+, O^+, O^{++}, O_2^+). Among the positive ions, H^+ and O^+ are seen to be most prominent with number density almost equal to electron number density. As it can be seen from the Fig. 5(*a*), the positive charge of the plasma due to presence of positive ions is mostly compensated by electrons ensuring a quasi-neutral plasma. As the number of reactions generating negative ions are limited, the number density of negative ions (H^-, O^-, OH^-) is nearly constant throughout the discharge. Among the negative ions, H^- is seen to be most prominent with number density of $\approx 10^{24}$ m^{-3}. Comparing number densities of all the species irrespective of their charge, atomic hydrogen (H) has the highest density for first couple of microseconds, which then combines at the wall surface to form hydrogen molecule (H_2). As the density of H decreases, density of H_2 increases which forms significant portion of the plasma after $t \approx 2$ μs along with O and O_2.

Due to expansion of the plasma bubble, radiation and heat transfer to the walls, the electron temperature (T_e) as well as the ion-neutral temperature (T_e) decreases over the discharge duration as shown in Fig. 5(*b*). It should be noted that due to the energy exchange via elastic scattering between electrons and neutrals, and via Coloumb interaction between electrons and ions; T_e and T_g very closely follow each other almost throughout the discharge demonstrating thermal equilibrium in the plasma. As seen from Table 4, the electrons and the other species share the common plasma temperature ($T = T_e = T_g$) in a typical μ-EDM with a time-averaged value of 14,794 K.

From manufacturing point of view, the most important consequence of the μ-EDM plasma is the heat flux transferred by the plasma to the electrodes during the discharge, which is plotted in Fig. 5(*e*). The total heat flux to the workpiece (anode) is a combination of the raditiative heat flux and the heat flux due to bombardment of electrons onto the workpiece surface. Similarly, the total heat flux to the tool electrode (cathode) is contributed by the radiative heat flux and bombardment of positive ions. It is seen that the heat flux to the anode is greater than the heat flux to the cathode during the initial few hundreds of nanoseconds. However, as the time progresses, the heat flux to both the electrons is found to be almost equal. The time-averaged value of the heat flux to the workpiece (anode) in the typical μ-EDM discharge is found to be 9.44×10^{10} W/m^2, while time-averaged heat flux to the cathode is 3.90×10^{10} W/m^2.

4.2 Effect of Applied Electric Field and Gap Distance on Plasma Characteristics. To study the effect of applied electric field and the interelectrode gap distance on the discharge characteristics, simulation experiments are conducted with eight levels of applied electric field and eight levels of the gap distance. The levels for these parameters are chosen so as to cover a wide range of field and gap values typically used in μ-EDM and are tabulated in Table 5. While running the simulations at constant input electric field, the maximum current is fixed at $I \leq I_{max}$ as in current-limited power supplies commonly used for the μ-EDM. In this study, $I_{max} = 20$ A is chosen.

During the simulation trials, it was seen that for some of the combinations of the electric field and gap, the initial electron density drops to almost zero value before the discharge is complete, causing numerical instability of the solver. Figure 6 shows the domain of the applied voltage and discharge gap levels. The combinations of electric field (E) and gap (L) for which the evolution of plasma is successfully simulated using the model are

Table 5 Levels of electric field and gap used for simulation experiments

Process parameter	Levels
Electric field (MV/m)	10, 25, 50, 100, 200, 500, 1000, 2000
Gap (μm)	0.5, 1, 2, 3, 4, 5, 10, 20

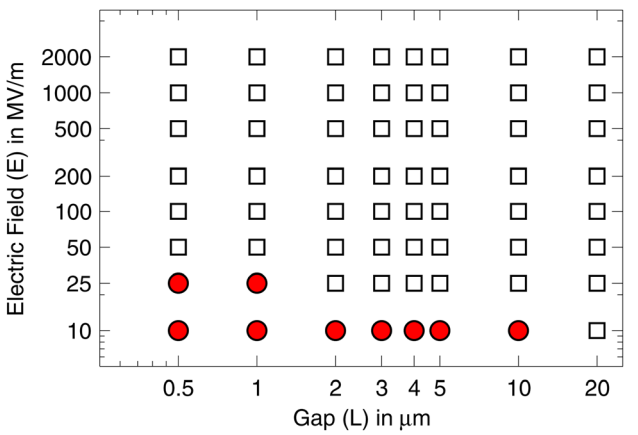

Fig. 6 Electric field (*E*)–Gap (*L*) domain of the μ-EDM plasma model (square represents point is [*E, L*] domain where discharge was successfully simulated, and circle represents failure of the model in obtaining plasma evolution at point [*E, L*])

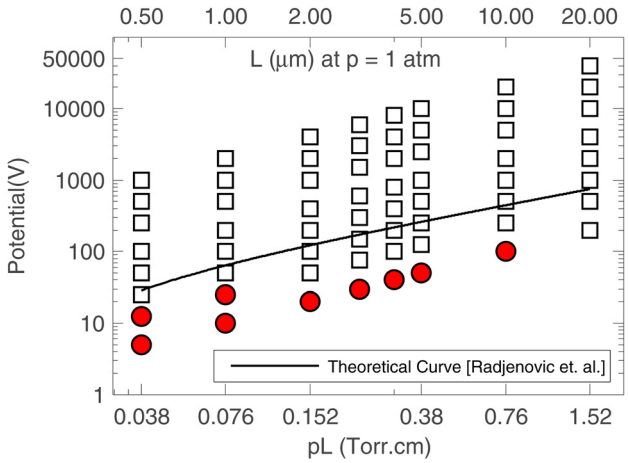

Fig. 7 Paschen like curve for H_2O using μ-EDM plasma model (square represents point is [*V, pL*] domain where discharge was successfully simulated, and circle represents failure of the model in obtaining plasma evolution at point [*V, pL*])

indicated by squares, whereas the combinations of (E, L) for which the model fails to predict evolution of plasma are indicated by circles. It can be seen from the figure that the discharge in deionized water is not sustained below a threshold electric field at each gap distance. This behavior of the deionized water can be explained using the Paschen law, which governs the minimum breakdown potential (V) between two electrodes at different pressures (p) and interelectrode gaps (L). The similarity of the curve in Fig. 6 with the Paschen curve for water is investigated, first, by converting the curve into V versus pL curve (see Fig. 7) and then, comparing it with the empirical relation obtained in a theoretical study of breakdown of water vapor by Radjenović et al. [27]. The pressure is assumed to be 1 atmospheric pressure.

As seen from Fig. 7, the minimum breakdown potential predicted by the model for a given gap closely follows the theoretical curve of breakdown potential versus gap distance reported in Ref. [27] for gap distances in the range of 0.5–15 μm at atmospheric pressure. It has been shown previously [28,29] that the global model approach can be used to successfully predict the breakdown phase of a discharge. Figure 7 indicates that the minimum breakdown potential increases as the interelectrode gap is

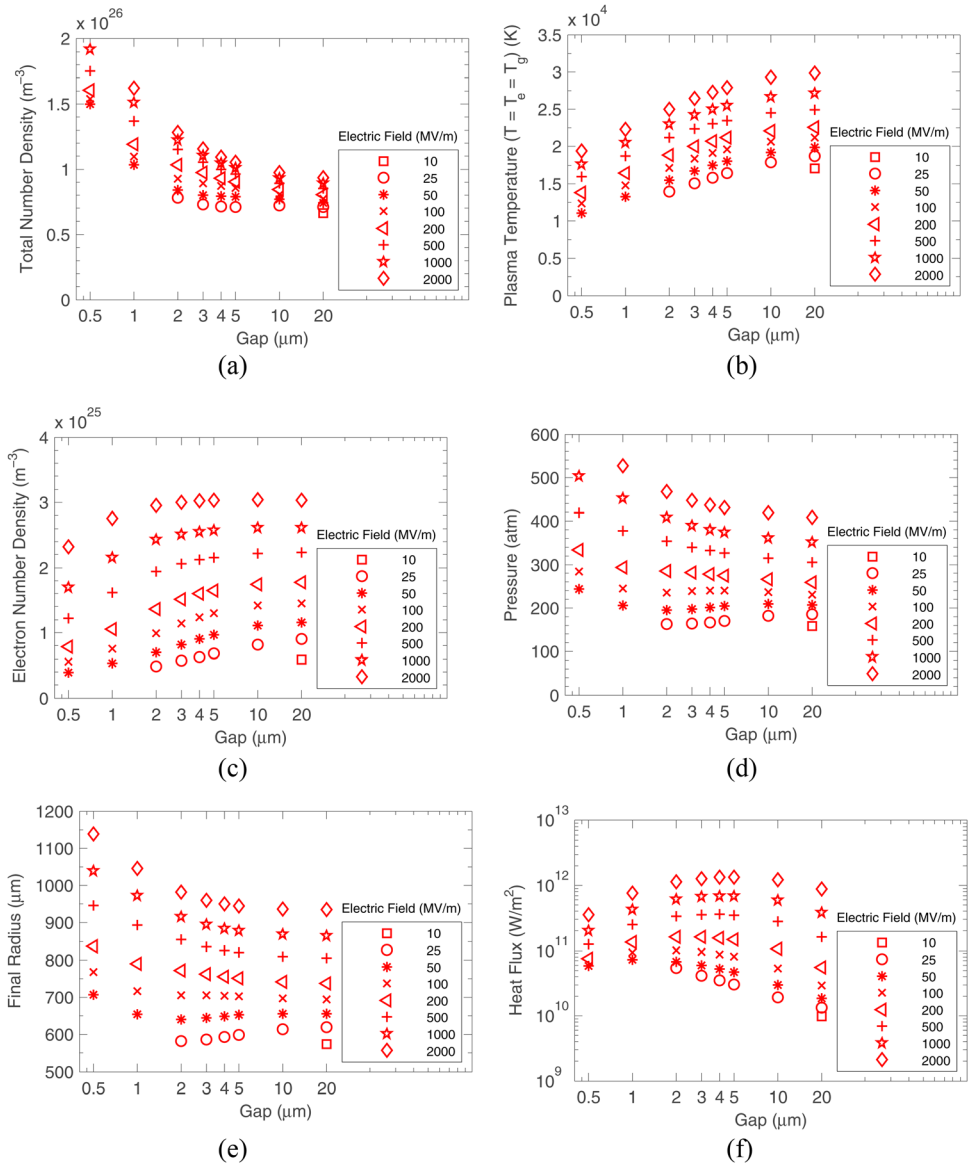

Fig. 8 Effect of applied electric field and discharge gap on the time-averaged plasma characteristics, namely, total plasma density, plasma temperature, electron density, plasma pressure, final plasma radius, and heat flux to workpiece

increased keeping the pressure constant. It should be noted that the minimum breakdown potential for a given gap also depends on the initial conductivity of the DI water, which is proportional to initial electron population (refer to Eq. (11)). For lower initial electron population, the minimum breakdown potential is higher for a given gap.

To analyze the effect of electric field and the gap distance, time-averaged electron density, time averaged-common plasma temperature ($T = T_e = T_g$) temperature, final plasma radius, time-averaged plasma pressure, and time-averaged heat flux are plotted for different values of electric field and gap distance as shown in Fig. 8. Figure 8(*a*) presents the effect of the electric field and the gap on time-averaged plasma density, i.e., the combined density of all the species in the plasma during the discharge. As seen from the figure, application of higher electric field at a given gap distance results in increase in the overall density of the plasma due to increase in the input electrical power that goes into the discharge. However, for a fixed value of electric field, increase in the gap distance results in decrease in the overall plasma density due to larger plasma volume. The variation of the plasma density over the simulation trials is seen to be within an order of magnitude. Effect of the electric field and gap on the common plasma temperature is shown in Fig. 8(*b*). As the electrical power input to the plasma is proportional to the square of the applied electric field (Eq. (10)), increase in the value of electric field for a given gap results in higher plasma temperature. Similarly, increasing the gap distance for a fixed value of electric field increases the plasma temperature. For fixed value of the electric field, Eqs. (10) and (11) imply that the input electrical power is independent of the volume of the plasma, therefore, independent of the gap distance. However, the overall plasma density decreases with the gap distance. Thus, the same input power is now distributed over fewer plasma particles giving rise to increase in the plasma temperature.

Figure 8(*c*) presents how time-averaged electron density in the plasma varies with the electric field and gap values. It is seen that the electron density follows similar trend as the plasma temperature showing increase with increase in the electric field and/or the gap distance. This can be explained using Fig. 3, which indicates that at higher plasma temperatures ionization reactions generating electrons have higher reactions rates than the recombination reactions in which the electrons are consumed. The plasma pressure depends on both, the plasma density and the plasma temperature under assumption of the ideal gas law ($p = NkT/V$). As higher electric field at a given gap results in increase in both, the plasma density and temperature, the plasma pressure increases with increase in the electric field as shown in Fig. 8(*d*). However, for a fixed value of electric field, the plasma density decreases with the gap distance, while the plasma temperature increased with the gap distance. As a result, the plasma pressure decreases with the increase in gap for electric fields above 100 MV/m, but increases with the increase in gap for electric fields below 100 MV/m and gaps between 2–20 μm. The velocity of expansion of radius of the plasma depends directly on the pressure inside the plasma bubble. Therefore, for same initial value of plasma radius, the final radius (R at $t = 5$ μs) is larger for higher plasma pressure as seen in Fig. 8(*e*). Therefore, the effect of electric field and gap on the final radius of the plasma follows similar trend as the plasma pressure. Finally, Fig. 8(*f*) is presented to demonstrate the effect of applied electric field and gap on the time-averaged heat flux transferred to the workpiece during the discharge. The heat flux is given by the addition of power transferred by the electrons at the workpiece surface per unit area and the radiation. Therefore, the value of the heat flux depends on the electron density and plasma temperature. As seen from Fig. 8(*f*), higher field results in a greater heat flux. With increase in gap, however, the heat flux increases initially for gaps up to 3 μm and then starts decreasing.

Note that the heat flux and the pressure exerted by the plasma are the two key parameters that cause the material removal from the workpiece during each discharge event. By knowing the evolution of heat flux and pressure during a single μ-EDM discharge as predicted by the model, volume of the workpiece material removed per discharge can be calculated by a melt-pool model using a coupled system of Navier–Stokes equation and heat equation. Heat flux predicted by the model appears as the heat source term in the heat equation, while the pressure force exerted by the plasma appears as a body force term in the Navier–Stokes equation. To obtain a complete description of a single μ-EDM discharge event including the material removal, the plasma model presented in this paper can be coupled with the melt-pool model.

5 Conclusions

This paper explains development of a spatially uniform model of μ-EDM plasma discharge in deionized water. The plasma discharge was modeled using a coupled system of particle balance equation, energy balance equation, and the plasma bubble dynamics. Using chemistry of H_2O plasma, number densities of different species in the plasma are estimated as a function of time using the particle balance equation. Time evolution of the plasma temperature is given by solving two separate energy balance equations for two separate temperatures, one for electrons and another for ensemble of ions and neutrals. It is shown that the electrons and ions/neutrals attain thermal equilibrium via energy exchange to reach a common plasma temperature. Expansion of plasma bubble is modeled by the plasma dynamics following Kirkwood-Bethe equation. Using the model, a single discharge of a typical μ-EDM process is simulated in order to obtain complete temporal description of the plasma characteristics. Further, simulation experiments are carried out to investigate effect of applied electric field and interelectrode gap distance on the μ-EDM plasma. Specific conclusions of the research are noted as follows:

(1) The μ-EDM plasma model is used to predict the characteristics of the plasma as a function of time. Plasma is characterized by the number densities of different species in the plasma, temperature of the plasma, radius, and velocity of the plasma bubble, pressure of the plasma bubble as well as the heat flux transferred to the workpiece during the discharge process.
(2) The model is validated using the experimental results reported by Nagahanumaiah et al. [25]. For experimental conditions of the referred study, the model predicts average electron temperature of 6817 K and electron density of 8.9×10^{23} m^{-3} against average electron temperature of 6217 K and electron density of 23.9×10^{23} m^{-3} reported in Ref. [25]. Furthermore, the values of electron temperature and density predicted by the model are found to be consistent with the range of electron temperature and density (5000–10,000 K, 10^{23}–10^{25} m^{-3}) reported in the literature [6,8,25,30].
(3) Application of higher field at a fixed gap increases the electron density, plasma temperature, plasma radius, plasma pressure and the heat flux to the workpiece, while increasing gap distance for a fixed electric field results in decrease of overall plasma density and increased heat flux. At fixed electric field, plasma pressure and radius decrease when the gap is increased when electric field is greater than 100 MV/m, but increase when the electric field is below 100 MV/m.
(4) The results of heat flux and pressure predicted by the plasma model can be used to develop a workpiece melt-pool model consisting Navier–Stokes equation coupled with the heat equation. Using the melt-pool model, material removal mechanism in μ-EDM process can be understood and volume of the material removed can be estimated.

Acknowledgment

This material is based in part upon work supported by the National Science Foundation under Award No. 1033362. The authors are grateful to NSF for funding this research.

Appendix

Table 6 Plasma reactions and corresponding reaction rates in the form $a * T^b * \exp(c * T^d)$ [17,18]

Reaction	a	b	c	d	E_{th}
$e^- + H_2O \rightarrow e^- + H_2O$				$f(T_e)$ [17]	
$e^- + H_2O \rightarrow e^- + e^- + H_2O^+$				$f(T_e)$ [17]	13.5
$e^- + H_2O \rightarrow e^- + e^- + H + OH^+$				$f(T_e)$ [17]	18.116
$e^- + H_2O \rightarrow O^+ + H_2 + e^- + e^-$				$f(T_e)$ [17]	19
$e^- + H_2O \rightarrow e^- + e^- + H^+ + OH$				$f(T_e)$ [17]	16.9
$e^- + H_2O \rightarrow O + H_2^+ + e^- + e^-$				$f(T_e)$ [17]	20.7
$e^- + H_2O \rightarrow H + OH + e^-$				$f(T_e)$ [17]	
$e^- + H_2O \rightarrow H^- + OH$				$f(T_e)$ [17]	
$e^- + H_2O \rightarrow H_2 + O^-$				$f(T_e)$ [17]	
$e^- + H_2O \rightarrow OH^- + H$				$f(T_e)$ [17]	
$H_2O^+ + H_2O \rightarrow H_3O^+ + OH$	2.10×10^{-15}	0	0	0	
$OH^+ + H_2O \rightarrow H_3O^+ + O$	1.30×10^{-15}	0	0	0	
$e^- + H_3O^+ \rightarrow H_2O + H$	1.74×10^{-14}	−0.5	0	0	
$e^- + H_3O^+ \rightarrow OH + H + H$	4.15×10^{-14}	−0.5	0	0	
$e^- + OH \rightarrow e^- + e^- + OH^+$	1.99×10^{-16}	1.78	−13.8	−1	12.95
$e^- + OH \rightarrow e^- + O + H$	2.08×10^{-13}	−0.76	−6.91	−1	
$e^- + OH^+ \rightarrow e^- + O + H^+$	1.64×10^{-10}	−2.04	−15.1	−1	
$e^- + H_2 \rightarrow e^- + e^- + H_2+$	1.03×10^{-14}	1.61	−17.9	−1	15.43
$e^- + H_2 \rightarrow e^- + H + H$	2.51×10^{-13}	−0.8	−10.9	−1	
$e^- + H_2+ \rightarrow e^- + H^+ + H$	1.79×10^{-13}	−0.87	−6.92	−1	
$H + H + H \rightarrow H_2 + H$	1.55×10^{-46}	−1	0	0	
$H + H + H_2 \rightarrow H_2 + H_2$	1.55×10^{-46}	−1	0	0	
$O + OH \rightarrow H + O_2$	3.74×10^{-17}	0.28	0	0	
$H + H + OH \rightarrow H_2O + H$	4.61×10^{-46}	−2	0	0	
$e^- + H \rightarrow e^- + e^- + H^+$	7.78×10^{-15}	0.41	−13.6	−1	13.6
$e^- + e^- + H^+ \rightarrow H + e^-$	6.38×10^{-43}	1.09	0	0	
$e^- + O \rightarrow e^- + e^- + O^+$	1.57×10^{-14}	0.43	−14.75	−1	13.62
$e^- + e^- + O^+ \rightarrow O + e^-$	2.59×10^{-42}	−1.07	−1.13	−1	
$e^- + O^+ \rightarrow e^- + e^- + O^{++}$	5.87×10^{-15}	0.41	−36.84	−1	35.12
$e^- + e^- + O^{++} \rightarrow O^+ + e^-$	9.72×10^{-43}	−1.09	−1.72	−1	
$e^- + O^{++} \rightarrow e^- + e^- + O^{+++}$	2.02×10^{-15}	0.45	−55.94	−1	54.94
$e^- + e^- + O^{+++} \rightarrow O^{++} + e^-$	3.35×10^{-43}	−1.05	−1	−1	
$e^- + O_2 \rightarrow e^- + O + O$	5.72×10^{-16}	0.5	−8.4	−1	
$O_2 + O_2 \rightarrow O + O + O_2$	5.80×10^{-15}	−0.83	−5.12	−1	
$O_2 + O \rightarrow O + O + O$	1.30×10^{-14}	−1	−5.12	−1	
$O + O + O_2 \rightarrow O_2 + O_2$	8.60×10^{-46}	−0.33	0	0	
$O + O + O \rightarrow O_2 + O$	1.90×10^{-45}	−0.5	0	0	
$e^- + e^- + H_2O^+ \rightarrow H_2O + e^-$	4.92×10^{-42}	−1.27	−6	−1	
$e^- + O_2 \rightarrow e^- + e^- + O_2+$	1.27×10^{-15}	1.36	−11.41	−1	12.1
$e^- + O_2+ \rightarrow O + O$	2.10×10^{-14}	−0.5	0	0	
Surface reactions	Probability				
$H + H \rightarrow H_2$	3.00×10^{-02}				
$O + O \rightarrow O_2$	2.00×10^{-02}				

References

[1] Dhanik, S., and Joshi, S. S., 2005, "Modeling of a Single Resistance Capacitance Pulse Discharge in Micro-Electro Discharge Machining," ASME J. Manuf. Sci. Eng., **127**(4), pp. 759–767.

[2] Heuvelman, H. J., Horsten, J. A., and Veenstra, P. C., 1971, "An Introductory Investigation of Breakdown Mechanism in Electro-Discharge Machining," CIRP Ann., **20**(1), pp. 43–44.

[3] Jones, H. M., and Kunhardt, E. E., 1995, "Development of Pulsed Dielectric Breakdown in Liquids," J. Phys. D: Appl. Phys., **28**, pp. 178–188.

[4] Eckman, P. K., and Williams, E. M., 1960, "Plasma Dynamics in an Arc Formed by Low-Voltage Sparkover of a Liquid Dielectric," Appl. Sci. Res., Sec. B, **8**(1), pp. 299–320.

[5] Eubank, P. T., Patel, M. R., Barrufet, M. A., and Bozkurt, B., 1993, "Theoretical Models of the Electrica Discharge Machining the Variable Mass, Cylindrical Plasma Model," J. Appl. Phys., **73**(11), pp. 7900–7909.

[6] Descoeudres, A., Hollenstein, C., Wälder, G., Demellayer, R., and Perez, R., 2008, "Time- and Spatially-Resolved Characterization of Electrical Discharge Machining Plasma," Plasma Sources Sci. Technol., **17**(2), p. 024008.

[7] Kojima, A., Natsu, W., and Kunieda, M., 2008, "Spectroscopic Measurement of Arc Plasma Diameter in EDM," CIRP Ann. – Manuf. Technol., **57**(1), pp. 203–207.

[8] Kunieda, M., Lauwers, B., Rajurkar, K., and Schumacher, B., 2005, "Advancing EDM Through Fundamental Insight Into the Process," CIRP Ann. – Manuf. Technol., **54**(2), pp. 64–87.

[9] Lieberman, M. A., and Lichtenberg, A. J., 2005, *Principles of Plasma Discharges and Material Processing*, Wiley, New York.

[10] Ashida, S. C. L., and A. L. M., 1995, "Spatially Averaged (Global) Model of Time Modulated High Density Argon Plasmas," J. Vac. Sci. Technol. A, **13**(5), pp. 2498–2507.

[11] Meyyappan, R., and Govindan, T. R., 1995, "Modeling of Electron Cyclotron Resonance Discharges," IEEE Trans. Plasma Sci., **23**(4), pp. 623–627.

[12] Hockenberry, T. O., and Everard, W. M., 1967, "Dynamic Evolution of Events Accompanying the Low-Voltage Discharges Employed in EDM," IEEE Trans. Ind. General Appl., **I**, pp. 302–309.

[13] Watson, P. K., Chadband, W. G., and Mak, W. Y., 1985, "Bubble Growth Following a Localized Electrical Discharge Triggred Spark Gaps in Liquids," IEEE Trans. Electric. Insulation, **EI-20**(2), pp. 275–280.

[14] Lieberman, M. A., and Ashida, S., 1996, "Global Models of Pulse-Power-Modulated High-Density, Low-Pressure Discharges," Plasma Sources Sci. Technol., **5**, pp. 145–158.

[15] Lee, C., and Lieberman, M. A., 1995, "Global Model of Ar, O2, Cl2, and Ar/O2 High-Density Plasma Discharges," J. Vac. Sci. Technol. A, **13**(2), pp. 368–380.

[16] Liu, D. X., Bruggeman, P., Iza, F., Rong, M. Z., and Kong, M. G., 2010, "Global Model of Low-Temperature Atmospheric-Pressure $He + H_2O$ Plasmas," Plasma Sources Sci. Technol., **19**(2), p. 025018.

[17] Itikawa, Y., and Mason, N., 2005, "Cross Sections for Electron Collisions With Water Molecules," J. Phys. Chem. Ref. Data, **34**(1), p. 1.

[18] Gordon, D. F., Helle, M. H., and Jones, T. G., 2012, *CHMWTR: A Plasma Chemistry Code for Water Vapor*, Plasma Physics Division, Naval Research Laboratory, Washington, DC.
[19] Huba, J. D., 2011, *NRL Plasma Formulary*, Naval Research Laboratory, Washington, DC.
[20] Nagaraja, S., Yang, V., and Adamovich, I., 2013, "Multi-Scale Modelling of Pulsed Nanosecond Dielectric Barrier Plasma Discharges in Plane-to-Plane Geometry," J. Phys. D: Appl. Phys., **46**(15), p. 155205.
[21] Roberts, R. M., Cook, J. A., and Rogers, R. L., 1996, "The Energy Partition of Underwater Sparks," J. Acoust. Soc. Am., **99**(6), pp. 3465–3475.
[22] Cook, J. A., Gleeson, A. M., Roberts, R. M., and Rogers, R. L., 1997, "A Spark-Generated Bubble Model With Semi-Empirical Mass Transport," J. Acoust. Soc. Am., **101**(4), pp. 1908–1920.
[23] Conductivity Guide, http://www.vl-pc.com/index.cfm/technical-info/conductivity-guide/, last accessed Dec 1, 2013
[24] Water Thermal Properties, http://www.engineeringtoolbox.com/water-thermal-properties-d_162.html, last accessed Dec 1, 2013
[25] Nagahanumaiah, Janakarajan, R., Glumac, N., Kapoor, S. G., and DeVor, R. E., 2009, "Characterization of Plasma in Micro-EDM Discharge Using Optical Spectroscopy," J. Manuf. Process., **11**(2), pp. 82–87.
[26] Lu, X., Kolb, J. F., Xiao, S., Laroussi, M., and Schoenbach, K. H., 2005, "Dielectric Strength of Sub-Millimeter Water Gaps Subjected to Microsecond and Sub-Microsecond Voltage Pulses," IEEE Pulsed Power Conference, pp. 600–603.
[27] Radjenović, M. R., Radjenovic, B., and Savic, M., 2010, "Breakdown Phenomena in Water Vapor Microdischarges," Acta Phys. Polon. A, **117**(5), pp. 752–755.
[28] Nam, S. K., and Verboncoeur, J. P., 2008, "Global Model for High Power Microwave Breakdown at High Pressure," Proceedings of the 2008 IEEE International Power Modulators and High Voltage Conference, **1253**, pp. 564–566.
[29] Nam, S. K., Lim, C., and Verboncoeur, J. P., 2009, "Dielectric Window Breakdown in Oxygen Gas: Global Model and Particle-in-Cell Approach," Phys. Plasmas, **16**(2), p. 023501.
[30] Heinz, K., Kapoor, S. G., DeVor, R. E., and Surla, V., 2011, "An Investigation of Magnetic-Field-Assisted Material Removal in Micro-EDM for Nonmagnetic Materials," ASME J. Manuf. Sci. Eng., **133**(2), p. 021002.